

Strain dependence of Berry-phase-induced anomalous Hall effect in the non-collinear antiferromagnet Mn_3NiN

Cite as: Appl. Phys. Lett. **119**, 222401 (2021); <https://doi.org/10.1063/5.0072783>

Submitted: 24 September 2021 • Accepted: 11 November 2021 • Published Online: 29 November 2021

Published open access through an agreement with Imperial College London

 F. Johnson,  D. Boldrin,  J. Zemen, et al.

COLLECTIONS

 This paper was selected as an Editor's Pick



View Online



Export Citation



CrossMark

ARTICLES YOU MAY BE INTERESTED IN

[Room temperature anomalous Hall effect in antiferromagnetic \$\text{Mn}_3\text{SnN}\$ films](#)

Applied Physics Letters **117**, 222404 (2020); <https://doi.org/10.1063/5.0032106>

[Electrical current switching of the noncollinear antiferromagnet \$\text{Mn}_3\text{GaN}\$](#)

Applied Physics Letters **115**, 052403 (2019); <https://doi.org/10.1063/1.5109317>

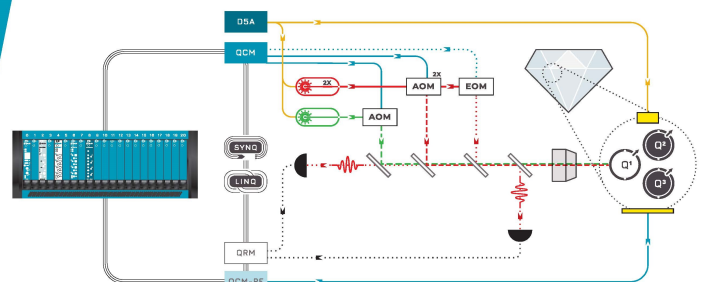
[Anomalous Hall effect in thin films of the Weyl antiferromagnet \$\text{Mn}_3\text{Sn}\$](#)

Applied Physics Letters **113**, 202402 (2018); <https://doi.org/10.1063/1.5064697>

 QBLOX

Integrates all
Instrumentation + Software
for Control and Readout of
NV-Centers

visit our website >



Strain dependence of Berry-phase-induced anomalous Hall effect in the non-collinear antiferromagnet Mn_3NiN

Cite as: Appl. Phys. Lett. **119**, 222401 (2021); doi: [10.1063/5.0072783](https://doi.org/10.1063/5.0072783)

Submitted: 24 September 2021 · Accepted: 11 November 2021 ·

Published Online: 29 November 2021




View Online



Export Citation



CrossMark

F. Johnson,^{1,a)}  D. Boldrin,^{1,2}  J. Zemen,³  D. Pesquera,⁴  J. Kim,⁴  X. Moya,⁴  H. Zhang,⁵  H. K. Singh,⁵  I. Samathrakris,⁵ and L. F. Cohen¹ 

AFFILIATIONS

¹Blackett Laboratory, Imperial College, Prince Consort Rd., London SW7 2AZ, United Kingdom

²SUPA, School of Physics and Astronomy, University of Glasgow, Glasgow G12 8QQ, United Kingdom

³Faculty of Electrical Engineering, Czech Technical University in Prague, Technicka 2, Prague 166 27, Czech Republic

⁴Department of Materials Science, University of Cambridge, 27 Charles Babbage Road, Cambridge CB3 0FS, United Kingdom

⁵Institute of Materials Science, TU Darmstadt, 64287 Darmstadt, Germany

^{a)}Author to whom correspondence should be addressed: fj214@ic.ac.uk

ABSTRACT

The anomalous Hall effect (AHE) has been shown to be present in certain non-collinear antiferromagnets due to their symmetry-breaking magnetic structure, and its magnitude is dependent primarily on the non-zero components of the Berry curvature. In the non-collinear antiferromagnet Mn_3NiN , the Berry phase contribution has been predicted to have strong strain dependence, although in practice, direct observation may be obscured by other strain-related influences—for instance, magnetic phase transitions mediated by strain. To unravel the various contributions, we examine the thickness and temperature dependence of the AHE for films grown on the piezoelectric substrate BaTiO_3 . We observe a systematic reduction in T_N due to increased compressive strain as film thickness is reduced and a linear decrease in the AHE magnitude as the films are cooled from their ferrimagnetic phase above T_N to their antiferromagnetic phase below. At 190 K, we applied an electric field across a 0.5 mm thick BaTiO_3 substrate with a 50 nm thick Mn_3NiN film grown on top and we demonstrate that at the coercive field of the piezoelectric substrate, the tensile in-plane strain is estimated to be of the order of 0.15%, producing a 20% change in AHE. Furthermore, we show that this change is, indeed, dominated by the intrinsic strain dependence of the Berry curvature.

© 2021 Author(s). All article content, except where otherwise noted, is licensed under a Creative Commons Attribution (CC BY) license (<http://creativecommons.org/licenses/by/4.0/>). <https://doi.org/10.1063/5.0072783>

The field of antiferromagnetic (AFM) spintronics has seen intense activity due to increased focus on the class of non-collinear AFM materials—most often the family of hexagonal Mn_3X (where $\text{X} = \text{Sn, Ge, Ga}$) or antiperovskite cubic Mn_3Y (where $\text{Y} = \text{Ir, Pt}$). It is well known that the presence of non-collinear Mn moments lying in the kagome (0001) or (111) plane, respectively, leads to a Berry-phase boost in various physical properties. Predictions and observations include the giant anomalous Hall effect (AHE),¹ the sizable anomalous Nernst effect (ANE),² the magneto-optical Kerr effect (MOKE),^{3–5} and the planar Hall effect.⁶ More recent studies have investigated the AFM domain structure in thin films using the size dependence of the ANE and both the size and angular dependence of the AHE.^{7–10} In addition, a 10% change in the tunneling resistance has been achieved in AFM spintronic tunnel junction devices, using strain applied with a

piezoelectric substrate.¹¹ Such work is necessary for realizing viable AFM spintronic devices on the nanoscale, where their lack of sizable stray fields gives them a significant advantage over conventional ferromagnetic materials.^{12,13}

The related Mn_3AN family of antiperovskites (where $\text{A} = \text{Sn, Ni, Ga, etc.}$) has historically seen interest due to their anomalous thermal expansion¹⁴ and potentially useful barocaloric cooling properties,^{15,16} where active control using strain is desirable.¹⁷ More recently, it has been appreciated that these materials possess a magnetic order symmetry similar to Mn_3Y , shown to support the giant anomalous Hall effect (AHE), and predicted to show the sizable anomalous Nernst effect (ANE).^{18,19} The magnetic symmetry allows for non-zero piezomagnetism,^{20–22} attractive because the net magnetic moment of the material is linearly coupled to an applied strain at small strains. The

geometrically frustrated Mn–Mn magnetic interactions lead to non-collinear AFM order below the Néel temperature T_N where moments are constrained to the (111) plane and adopt the symmetry of the irreducible representations termed Γ^{4g} and Γ^{5g} (in the notation of Fruchart and Bertaut²³). Both structures are fully compensated and are related to each other by a 90° rotation of the Mn moments within the (111) plane. Recently, it has been shown that Mn_3GaN , with a T_N of ~ 300 K, can grow epitaxially on oxide perovskite substrates with an atomically sharp interfacial layer,²⁴ be switched by an applied spin torque,²⁵ and generate unconventional spin-Hall torque (with both in-plane and importantly out-of-plane components).²⁶

Here, we focus on Mn_3NiN , which has a lattice parameter $a = 3.887 \text{ \AA}$ and a first-order paramagnetic to AFM transition at $T_N = 235$ K in the target used to grow the films. This transition has been shown to be highly strain dependent, with T_N able to be varied by ± 30 K with $\pm 0.25\%$ in-plane biaxial strain.²⁷ The strain influences T_N by changing the lattice parameters, and therefore, the distance between the Mn sites, and the orientation of the spin on each Mn site, and hence, altering the exchange interaction. Furthermore, under compressive in-plane biaxial strain, the films support a soft ferrimagnetic phase above T_N , with a spin symmetry related to the Γ^{4g} structure.²⁸ Conventionally, the AHE is proportional to the total magnetization and so is not seen in AFM systems, but it is now accepted that AHE can arise through a combination of broken mirror symmetry (arising from the Γ^{4g} non-collinear magnetic structure) and spin-orbit coupling.¹⁹ These broken symmetries lead to a non-zero momentum space Berry curvature and an AHE.²² Therefore, although the unstrained Γ^{4g} magnetic configuration is fully compensated, a large AHE is possible because the symmetry requirements necessary for a Berry phase contribution to the AHE are satisfied. Strain effects on the anomalous Hall conductivity (AHC) are predicted to be large—a biaxial tensile in-plane strain that causes a distortion of the lattice parameters equivalent to a c/a ratio of 0.99 is predicted to enhance the AHC by 65%, while a biaxial tensile strain causing a c/a ratio of 1.01 reduces the AHC by 30%.¹⁸ Neutron diffraction has indicated that Mn_3NiN thin films have a Γ^{4g} component to their magnetic structure below T_N .²⁸ Films grown on $BaTiO_3$ (BTO) substrates show a sharp change in magnetization due to the effect of strain at the BTO structural transition at 187 K.²⁷ Active strain control of Mn_3AN , exploiting the piezoelectric properties of the BTO substrate directly, is so far lacking. Investigating whether the Berry curvature can be manipulated usefully is an important step toward exploring the potential of these versatile materials.

Mn_3NiN films in this study were grown at 400°C on single crystal (001)-oriented 0.5 mm thick BTO substrates, using pulsed laser deposition as described elsewhere.²⁷ The bulk lattice parameter of the Mn_3NiN target used for growth was 3.8805 \AA . Gold was deposited on the reverse side of the BTO using thermal evaporation, to act as a bottom electrode. To calculate the in-plane strain in Mn_3NiN films, it was assumed Poisson's ratio $\nu = 0.41$.²⁷ Four terminal magnetotransport data were collected in a square geometry using the van der Pauw method. Data were antisymmetrized to extract the Hall component. X-ray diffraction (XRD) was performed on a Malvern Panalytical Empyrean instrument with a sample stage where electric fields can be applied *in situ*. Software fits of the peaks were performed to extract the lattice parameters. Magnetic measurements to determine T_N were performed using the VSM option in a Quantum Design Physical Property Measurement System.

After the growth of the films at 400°C and subsequent cooling to room temperature, the BTO substrate entered the tetragonal phase unpoled. Figure 1(a) illustrates a typical “a” and “c” ferroelectric domain structure. A ferroelectric a domain refers to a region where the a-lattice parameter (3.987 \AA) is aligned with the out-of-plane direction, and likewise a c domain is where the c-lattice parameter (4.032 \AA) is aligned with the out-of-plane direction. At small electric fields, strain was applied from the BTO to the film through macroscopic 90° domain rotation. Due to the difference between the c-lattice parameter and the a-lattice parameter large strains can be generated. The initial c-domain volume fraction V_{002} was evaluated using the formula $V_{002} = (A_{002} \times 100) / (A_{002} + A_{200})$, where A denotes the area of the respective peak.

X-ray diffraction (XRD) was used at 300 K to measure, in the out-of-plane direction, both the 002 and 200 BTO substrate peaks [Fig. 1(b)] while an electric field, E , was applied out of the sample plane. Figure 1(c) shows the variation in the BTO c-axis lattice parameter with the applied field, with a butterfly figure hysteresis with an electric field.^{29,30} The behavior is consistent with a coercive field $E_c \approx 1 \text{ kV/cm}$, typical of BTO substrates,³¹ and at this coercive field, there is an out-of-plane compressive strain of -0.11% in the BTO.³² The substrate initially is majority c-axis oriented, but 90° domain reorientation also occurs in the BTO at E_c as shown in Fig. 1(d). In the vicinity of E_c the c-domain volume fraction, V_{002} changes by a maximum of 4.5%. Further increasing the electric field returns the substrate to a c-oriented state. This domain rotation generated a compressive strain out-of-plane (tensile in-plane) with a magnitude of $\sim -0.05\%$ ($+0.05\%$) at E_c .

The (111) kagome plane of the Mn_3NiN unit cell is shown schematically in Fig. 2(a), and the 002 Mn_3NiN film peak from a 100 nm thick film is shown in Fig. 2(b) as a function of an electric field. The dependence of the film c-lattice parameter with an electric field was extracted from these data [Fig. 2(c)]. The film is strain-coupled to the substrate and also has a characteristic butterfly loop shape with peaks

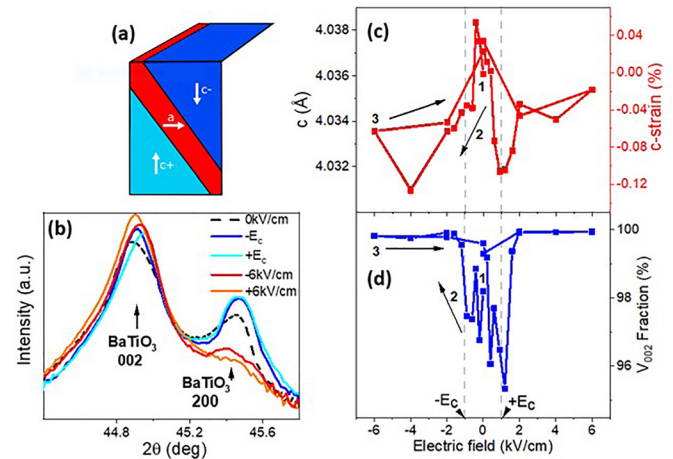


FIG. 1. (a) Schematic of the a–c domain structure present in the BTO substrate. Changes in out-of-plane x-ray diffraction with an electric field are shown on the BTO 002/200 peaks in (b). Changes in the 002/200 peak positions indicate changes in the lattice parameter, and the relative intensities show 90° domain reorientation. (c) The c lattice parameter shows a butterfly curve, with a behavior consistent with a coercive field $E_c = 1 \text{ kV/cm}$. The field sweep direction is shown with arrows. A change of approximately -0.12% strain occurs at E_c . (d) The c-domain volume fraction V_{002} changes by a maximum of 4.5% close to E_c .

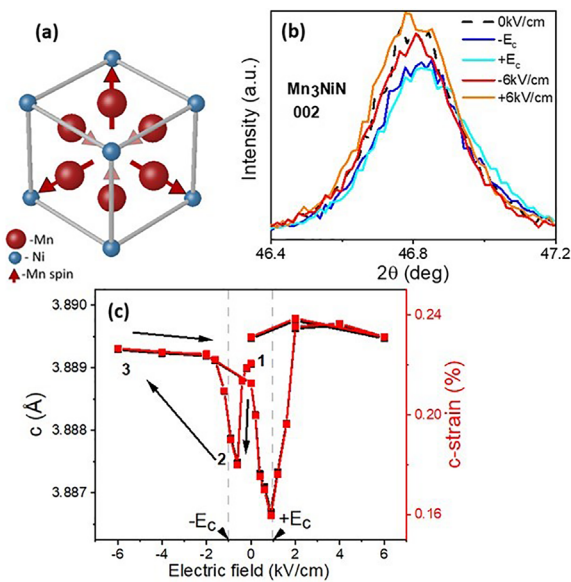


FIG. 2. (a) The antiperovskite crystal structure of Mn₃NiN viewed along the [111] direction, showing the Γ^{4g} magnetic structure. (b) Changes in out-of-plane x-ray diffraction with an electric field are shown on the film 002 peak. (c) Strain in the 100 nm Mn₃NiN film grown on BTO shows the expected “butterfly loop” shape with an applied electric field across the ferroelectric substrate, with -0.06% change in out-of-plane strain occurring at E_c . The strain change in the film is maximized at E_c , which corresponds to the highest proportion of a-domains and the biggest change in the c-lattice parameter.

at $E_c = \pm 1$ kV/cm. At $E = 0$ kV/cm, the film was under an average tensile out-of-plane strain of $+0.22\%$ (compressive in-plane of -0.090%) compared with the bulk polycrystalline target—this strain is due to growth on the lattice-mismatched BTO perovskite substrate. Increasing the electric field to E_c created tensile in-plane strain in the BTO, which was transferred to the film, and due to the Poisson effect, this reduced the out-of-plane strain to $+0.16\%$ (-0.065% in-plane). Further increasing the electric field up to the maximum applied field of 6 kV/cm released this compressive strain. Comparing this change to the maximum possible strain applied by the BTO gives a strain coupling efficiency of 38%, comparable to the 44% strain coupling efficiency reported previously.²⁷

In order to help quantify the relationship between strain and the anomalous Hall resistivity ρ_{xy} , Mn₃NiN films of thicknesses 20, 50, and 100 nm were grown on BTO. Figure 3(a) shows the saturation value $\rho_{xy,sat}(T)$, and Fig. 3(b) shows the extracted magnetic coercive fields H_c as a function of temperature. The inset to Fig. 3(c) shows a typical $\rho_{xy}(H)$ curve. For these films on BTO with compressive in-plane strain, ρ_{xy} is maximal in the ferrimagnetic phase above T_N and decreases quasi-linearly below T_N . Figure 3(c) shows that the thinner films, which are more highly strained, have a decreased T_N , but otherwise films of all thicknesses have very similar ρ_{xy} and $H_c(T)$ functional form. It has previously been reported that biaxial in-plane strains of $\pm 0.25\%$ caused a change in T_N of ± 30 K, from growth on (LaAlO₃)_{0.3}(Sr₂TaAlO₆)_{0.7} (LSAT) and SrTiO₃ (STO) substrates.²⁷ By measuring the in-plane strain of several Mn₃NiN films grown on BTO using XRD, and their T_N using magnetometry (see the [supplementary material](#), Fig. S4), we also observe a similar relationship when the strain is a function of film thickness [Fig. 3(c)].

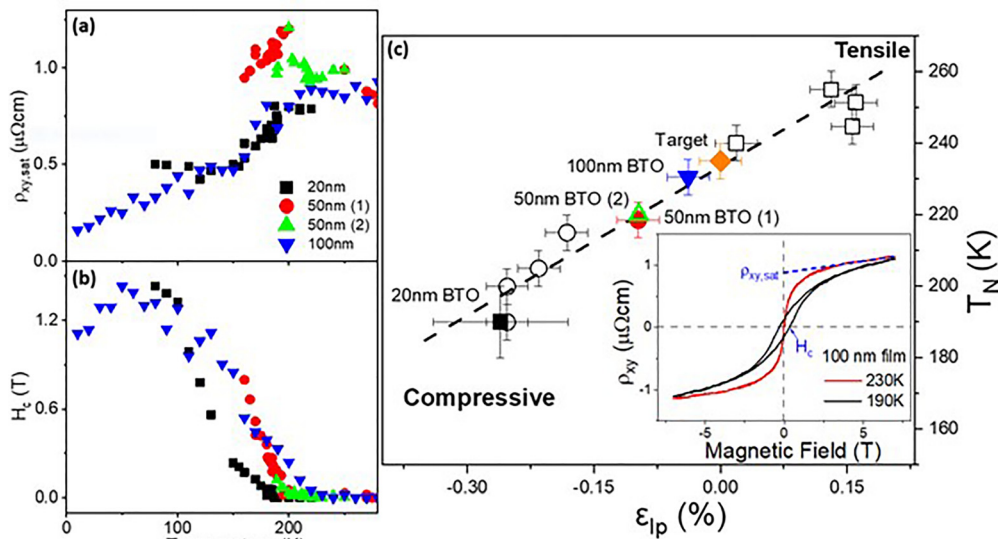


FIG. 3. (a) The dependence of the saturated anomalous Hall resistivity with temperature for Mn₃NiN films of varying thickness. (b) Coercive field measurements showing how T_N decreases with the decreasing film thickness. (c) T_N shows a linear dependence on in-plane (IP) strain in agreement with previous results for films grown on LSAT (open squares) and STO (open circles), reprinted with permission from Boldrin *et al.*, ACS Appl. Mater. Interfaces **10**, 18863 (2018). Copyright 2018 American Chemical Society. The dashed line shows the best fit to these data. The green triangle is the estimated strain for the sample measured in Fig. 4 based on its $T_N = 220$ K. Inset shows example anomalous Hall resistivity curves at 190 K (antiferromagnetic phase) and 260 K (ferrimagnetic phase) for the 100 nm thick film.

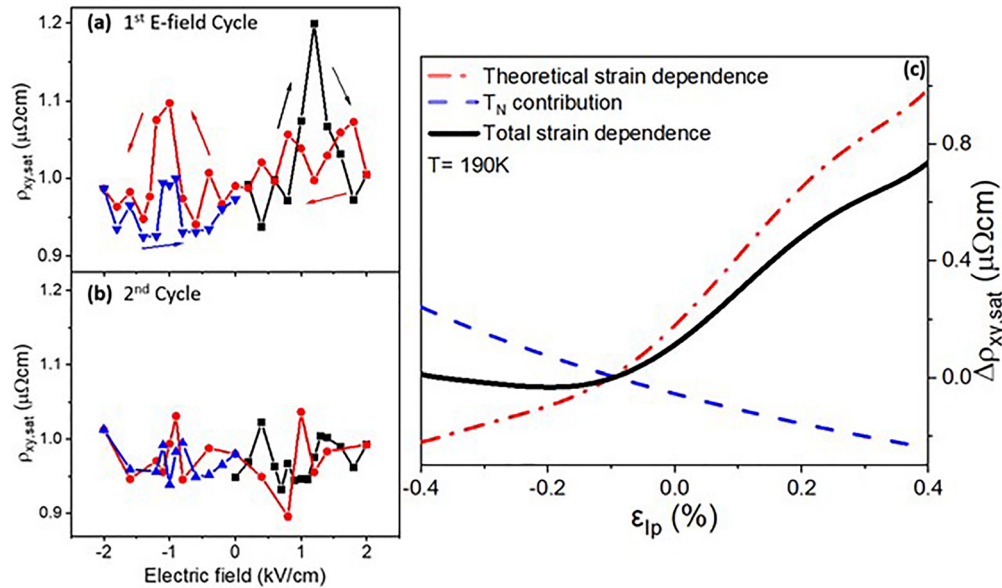


FIG. 4. (a) When an electric field is applied across a 50 nm Mn_3NiN film grown on BTO a boost of 20% to the anomalous Hall resistivity is observed in the vicinity of E_c . (b) The magnitude of this change decreases on subsequent E-field cycles. (c) The total strain dependence of the anomalous Hall resistivity is a sum of the intrinsic strain dependence of the Γ^{49} state and the dependence of T_N with strain. For a 50 nm film grown on BTO with initial strain -0.097% , the observed boost in (a) can be described by $+0.15\% \pm 0.01\%$ applied IP strain.

We performed magnetotransport measurements at 190 K on the 50 nm Mn_3NiN film on BTO, with active in-plane strain control achieved by applying an electric field across the film and substrate. At this temperature, BTO is in the orthorhombic phase, where $a \neq b \neq c$ due to a distortion of the unit cell along the $\langle 011 \rangle$ direction. This phase can be described in terms of a pseudomonoclinic lattice with $a_m = 3.983 \text{ \AA}$ and $b_m = c_m = 4.019 \text{ \AA}$.³⁵ This phase is also ferroelectric—large strain changes will occur when the electric field is in the vicinity of E_c and domains of differing orientations can form, giving a local compressive strain change out-of-plane of -0.9% .³⁴ In Fig. 4(a), it can be seen that at E_c , the saturated anomalous Hall resistivity was boosted by 20%, although subsequent electric field cycles [Fig. 4(b)] reduced the magnitude of this effect. Evidently from Fig. 3, active strain control with the sample sitting at a fixed bath temperature will manipulate ρ_{xy} , simply by virtue of the sensitivity of T_N to strain.

We have previously calculated the theoretical dependence of the Berry-phase contribution to anomalous Hall conductivity in Mn_3NiN ¹⁸ using maximally localized Wannier functions obtained by a projection of Bloch wave functions computed via the projector augmented wave method as implemented in the Vienna *Ab initio* Simulation Package (VASP) code.³⁵ Further details of the calculation are given in Ref. 18. The Berry-phase contribution was calculated as a function of the lattice parameters allowing estimate of the influence of strain on the intrinsic anomalous Hall. However, this linear response theory based on a zero-temperature ground state does not take into account the dependence of T_N on strain and the resulting influence on ρ_{xy} (T/T_N). From the study of films of different thicknesses shown in Fig. 3, tensile in-plane strain will increase T_N and, therefore, given the ρ_{xy} (T/T_N) dependence of these films, the strain dependence of T_N reduces the AHE magnitude in this case. Hence, for films on BTO substrates, there are two competing influences on the ρ_{xy} with active strain. The red dot-dash line in Fig. 4(c)

shows this first contribution, using the theoretical prediction from Ref. 18 of AHC converted to AHE resistivity using the relationship $\text{AHC} = \rho_{xy}/(\rho_{xx})^2$, and an experimental value for ρ_{xy} at the temperature of operation. The theoretical prediction was also modified to take into account changes in ρ_{xx} with strain (see the supplementary material, Fig. S3). The experimental data from Fig. 3 were used to construct the second contribution—the blue dash curve in Fig. 4(c). The dependence of ρ_{xy} with reduced temperature T/T_N was used in conjunction with the strain dependence of T_N to show how ρ_{xy} changes with strain from this contribution.

The sum of these two competing effects has been plotted as a solid black line in Fig. 4(c) to show the expected change in ρ_{xy} with strain for the 50 nm Mn_3NiN film at 190 K. From this figure, it is clear that ρ_{xy} is expected to be insensitive to in-plane strain when large compressive strain is applied, but under tensile strain, the intrinsic Berry-phase contribution dominates over the influence of T_N changes, and a large increase is expected. Using this summation curve, the increase in ρ_{xy} at E_c can be estimated to result from an in-plane tensile strain applied to the film of approximately $+0.15\%$. From the results of Ref. 27, this strain is also expected to reduce the net moment due to the piezomagnetic effect; however, in Ref. 18, we show that the large AHE in these films is dominated by the intrinsic component generated by the Berry curvature of the electronic band structure. Therefore, the overall dependence of the AHE on contribution of the net magnetic moment to the AHE is small. Repeated bipolar switching of the electric field is known to cause cracking in bulk ferroelectric materials due to stress generated at pinning sites.^{36–38} This fatigue reduced the magnitude of the strain generated in our sample and, therefore, the boost to ρ_{xy} decreased on subsequent cycles.

It is useful to review this performance in the context of other work on similar materials. In a recent report, it was shown that the non-collinear AFM to collinear AFM transition could be tuned by

25 K in the related system Mn_3Pt grown on BTO by applying an electric field of $E = 4 \text{ kV/cm}$ (at 360 K when the BTO is in its tetragonal phase).³⁹ However, the in-plane strain change achieved under this electric field was reported as -0.35% . The differences in the reported achievable strain compared to this report are due to the relative proportion of a to c domains present in the substrate, the temperature of the measurement, and the structural phase of the BTO at that temperature. In a study on Mn_3Ga films grown on piezoelectric $0.7\text{PbMg}_{1/3}\text{Nb}_{2/3}\text{O}_3-0.3\text{PbTiO}_3$ (PMN-PT), an applied electric field of 4 kV/cm caused an in-plane compressive strain of 0.1% , which decreased the AHE by 97% .¹¹ These changes are larger than those reported here, although further improvements are anticipated by fine-tuning the band structure through composition, in order to maximize the Berry curvature contribution.⁴⁰

The behavior of $\rho_{xy}(T)$ clearly diminishes the overall $\Delta\rho_{xy}$ achievable with strain for films grown on BTO. However, we have previously shown that films grown on $(\text{LaAlO}_3)_{0.3}(\text{Sr}_2\text{TaAlO}_6)_{0.7}$ (LSAT) substrates support very different $\rho_{xy}(T)$ behavior. The most significant difference is that the AHE is close to zero above T_N (due to an absence of the ferrimagnetic phase) and an increasing $\rho_{xy}(T)$ as temperature is decreased below T_N .^{18,27} The predicted composite strain change for Mn_3NiN on LSAT substrates (shown in Fig. S1) shows an encouraging future direction particularly for such films subjected to an external bending strain⁴¹ or using a buffer interfacial layer when growing on piezoelectric substrates to replicate initial tensile in-plane strain. Such an interfacial layer may also improve the mechanical properties as has been shown for Mn_3Sn growth on PMN-PT.⁴²

In conclusion, we have measured ρ_{xy} in thin films of Mn_3NiN grown on piezoelectric BTO substrates and have shown an active increase in ρ_{xy} in the AFM phase upon applying an electric field across the BTO at the coercive electric field of the substrate. This increase in ρ_{xy} cannot simply be described by changes in T_N due to strain and is attributed to the intrinsic strain dependence of the Berry-phase contribution due to the material's Γ^{4g} magnetic symmetry.

See the [supplementary material](#) for the theoretical dependence of $\rho_{xy,\text{sat}}$ with strain for Mn_3NiN grown on LSAT and for details of the calculation of ρ_{xx} with strain and temperature.

F.J. acknowledges funding from Hitachi Cambridge and F.J. and L.F.C. from the UK Engineering and Physical Sciences Research Council (EPSRC). D.P. acknowledges funding from the Agència de Gestió d'Ajuts Universitaris i de Recerca-Generalitat de Catalunya (Grant No. 2014 BP-A 00079). D.B. is grateful for support from a Leverhulme Trust Early Career Fellowship (No. ECF-2019-351) and a University of Glasgow Lord Kelvin Adam Smith Fellowship. X.M. is grateful for support from the Royal Society. The work of J.Z. was supported by the Ministry of Education, Youth and Sports of the Czech Republic from the OP RDE programme under the project International Mobility of Researchers MSCAIF at CTU No. CZ.02.2.69/0.0/0.0/18 070/0010457, and through the e-INFRA CZ (ID:90140). The authors acknowledge Joerg Wunderlich for useful discussions.

AUTHOR DECLARATIONS

Conflict of Interest

We have no conflicts of interest to disclose.

DATA AVAILABILITY

The data that support the findings of this study are available from the corresponding author upon reasonable request.

REFERENCES

- T. Higo, D. Qu, Y. Li, C. L. Chien, Y. Otani, and S. Nakatsuji, *Appl. Phys. Lett.* **113**, 202402 (2018).
- H. Narita, M. Ikhlas, M. Kimata, A. A. Nugroho, S. Nakatsuji, and Y. C. Otani, *Appl. Phys. Lett.* **111**, 202404 (2017).
- A. L. Balk, N. H. Sung, S. M. Thomas, P. F. S. Rosa, R. D. McDonald, J. D. Thompson, E. D. Bauer, F. Ronning, and S. A. Crooker, *Appl. Phys. Lett.* **114**, 032401 (2019).
- M. Wu, H. Isshiki, T. Chen, T. Higo, S. Nakatsuji, and Y. C. Otani, *Appl. Phys. Lett.* **116**, 132408 (2020).
- T. Higo, H. Man, D. B. Gopman, L. Wu, T. Koretsune, O. M. J. van't Erve, Y. P. Kabanov, D. Rees, Y. Li, M. Suzuki, S. Patankar, M. Ikhlas, C. L. Chien, R. Arita, R. D. Shull, J. Orenstein, and S. Nakatsuji, *Nat. Photonics* **12**, 73 (2018).
- L. Xu, X. Li, L. Ding, K. Behnia, and Z. Zhu, *Appl. Phys. Lett.* **117**, 222403 (2020).
- H. Bai, W. Zhu, Y. You, X. Chen, X. Zhou, F. Pan, and C. Song, *Appl. Phys. Lett.* **117**, 052404 (2020).
- H. Narita, T. Higo, M. Ikhlas, S. Nakatsuji, and Y. C. Otani, *Appl. Phys. Lett.* **116**, 072404 (2020).
- J. Yan, X. Luo, H. Y. Lv, Y. Sun, P. Tong, W. J. Lu, X. B. Zhu, W. H. Song, and Y. P. Sun, *Appl. Phys. Lett.* **115**, 102404 (2019).
- H. Iwaki, M. Kimata, T. Ikebuchi, Y. Kobayashi, K. Oda, Y. Shiota, T. Ono, and T. Moriyama, *Appl. Phys. Lett.* **116**, 022408 (2020).
- H. Guo, Z. Feng, H. Yan, J. Liu, J. Zhang, X. Zhou, P. Qin, J. Cai, Z. Zeng, X. Zhang, X. Wang, H. Chen, H. Wu, C. Jiang, and Z. Liu, *Adv. Mater.* **32**, 2002300 (2020).
- T. Jungwirth, X. Marti, P. Wadley, and J. Wunderlich, *Nat. Nanotechnol.* **11**, 231 (2016).
- Z. Liu, Z. Feng, H. Yan, X. Wang, X. Zhou, P. Qin, H. Guo, R. Yu, and C. Jiang, *Adv. Electron. Mater.* **5**, 1900176 (2019).
- M. Wu, C. Wang, Y. Sun, L. Chu, J. Yan, D. Chen, Q. Huang, and J. W. Lynn, *J. Appl. Phys.* **114**, 123902 (2013).
- D. Boldrin, E. Mendive-Tapia, J. Zemen, J. B. Staunton, T. Hansen, A. Aznar, J. L. Tamarit, M. Barrio, P. Lloveras, J. Kim, X. Moya, and L. F. Cohen, *Phys. Rev. X* **8**, 041035 (2018).
- D. Boldrin, E. Mendive-Tapia, J. Zemen, J. B. Staunton, A. M. Gomes, L. Ghivelder, J. Halpin, A. S. Gibbs, A. Aznar, J.-L. Tamarit, P. Lloveras, X. Moya, and L. F. Cohen, *Phys. Rev. B* **104**, 134101 (2021).
- B. Schleicher, R. Niemann, S. Schwabe, R. Hühne, L. Schultz, K. Nielsch, and S. Fähler, *Sci. Rep.* **7**, 14462 (2017).
- D. Boldrin, I. Samathrakris, J. Zemen, A. Mihai, B. Zou, F. Johnson, B. D. Esser, D. W. McComb, P. K. Petrov, H. Zhang, and L. F. Cohen, *Phys. Rev. Mater.* **3**, 094409 (2019).
- H. Chen, Q. Niu, and A. H. MacDonald, *Phys. Rev. Lett.* **112**, 017205 (2014).
- J. Zemen, Z. Gercsi, and K. G. Sandeman, *Phys. Rev. B* **96**, 024451 (2017).
- P. Lukashev, R. F. Sabirianov, and K. Belashchenko, *Phys. Rev. B* **78**, 184414 (2008).
- G. Gurung, D. F. Shao, T. R. Paudel, and E. Y. Tsymlal, *Phys. Rev. Mater.* **3**, 044409 (2019).
- D. Fruchart and E. F. Bertaut, *J. Phys. Soc. Jpn.* **44**, 781 (1978).
- C. X. Quintela, K. Song, D. F. Shao, L. X. T. Nan, T. R. Paudel, N. Campbell, X. Pan, T. Tybell, M. S. Rzechowski, E. Y. Tsymlal, S. Y. Choi, and C. B. Eom, *Sci. Adv.* **6**(30), eaba4017 (2020).
- T. Hajirra, S. Ishino, K. Matsuura, and H. Asano, *Appl. Phys. Lett.* **115**, 052403 (2019).
- T. Nan, C. X. Quintela, J. Irwin, G. Gurung, D. F. Shao, J. Gibbons, N. Campbell, K. Song, S. Y. Choi, L. Guo, R. D. Johnson, P. Manuel, R. V. Chopdekar, I. Hallsteinsen, T. Tybell, P. J. Ryan, J. W. Kim, Y. S. Choi, P. G. Radaelli, D. C. Ralph, E. Y. Tsymlal, M. S. Rzechowski, and C. B. Eom, *Nat. Commun.* **11**, 4671 (2020).
- D. Boldrin, A. P. Mihai, B. Zou, J. Zemen, R. Thompson, E. Ware, B. V. Neamtu, L. Ghivelder, B. Esser, D. W. McComb, P. Petrov, and L. F. Cohen, *ACS Appl. Mater. Interfaces* **10**, 18863 (2018).

- ²⁸D. Boldrin, F. Johnson, R. Thompson, A. P. Mihai, B. Zou, J. Zemen, J. Griffiths, P. Gubeljak, K. L. Ormandy, P. Manuel, D. D. Khalyavin, B. Ouladdiaf, N. Qureshi, P. Petrov, W. Branford, and L. F. Cohen, *Adv. Funct. Mater.* **29**, 1902502 (2019).
- ²⁹M. Oshiki and E. Fukada, *J. Mater. Sci.* **10**, 1–6 (1975).
- ³⁰R. Tazaki, D. Fu, M. Itoh, M. Daimon, and S. Koshihara, *J. Phys.* **21**, 215903 (2009).
- ³¹X. Moya, E. Stern-Taulats, S. Crossley, D. González-Alonso, S. Kar-Narayan, A. Planes, L. Mañosa, and N. D. Mathur, *Adv. Mater.* **25**, 1360 (2013).
- ³²H. H. Wieder, *J. Appl. Phys.* **26**, 1479 (1955).
- ³³G. H. Kwei, A. C. Lawson, S. J. L. Billinge, and S. W. Cheong, *J. Phys. Chem.* **97**, 2368 (1993).
- ³⁴R. V. Chopdekar and Y. Suzuki, *Appl. Phys. Lett.* **89**, 182506 (2006).
- ³⁵G. Kresse and J. Hafner, *Phys. Rev. B* **47**, 558 (1993).
- ³⁶C. S. Lynch, W. Yang, L. Collier, Z. Suo, and R. M. McMeeking, *Ferroelectrics* **166**, 11 (1995).
- ³⁷H. Wang and R. N. Singh, *Ferroelectrics* **168**, 281 (1995).
- ³⁸Z. Q. Liu, J. H. Liu, M. D. Biegalski, J.-M. Hu, S. L. Shang, Y. Ji, J. M. Wang, S. L. Hsu, A. T. Wong, M. J. Cordill, B. Gludovatz, C. Marker, H. Yan, Z. X. Feng, L. You, M. W. Lin, T. Z. Ward, Z. K. Liu, C. B. Jiang, L. Q. Chen, R. O. Ritchie, H. M. Christen, and R. Ramesh, *Nat. Commun.* **9**, 41 (2018).
- ³⁹Z. Q. Liu, H. Chen, J. M. Wang, J. H. Liu, K. Wang, Z. X. Feng, H. Yan, X. R. Wang, C. B. Jiang, J. M. D. Coey, and A. H. MacDonald, *Nat. Electron.* **1**, 172 (2018).
- ⁴⁰Y. Zhang, Y. Sun, H. Yang, J. Železný, S. P. P. Parkin, C. Felser, and B. Yan, *Phys. Rev. B* **95**, 075128 (2017).
- ⁴¹D. E. Parkes, S. A. Cavill, A. T. Hindmarch, P. Wadley, F. McGee, C. R. Staddon, K. W. Edmonds, R. P. Campion, B. L. Gallagher, and A. W. Rushforth, *Appl. Phys. Lett.* **101**, 072402 (2012).
- ⁴²X. Wang, Z. Feng, P. Qin, H. Yan, X. Zhou, H. Guo, Z. Leng, W. Chen, Q. Jia, Z. Hu, H. Wu, X. Zhang, C. Jiang, and Z. Liu, *Acta Mater.* **181**, 537 (2019).